Volume 26
Number 9
7 March 2024
Pages 1191–1340

CrystEngComm

rsc.li/crystengcomm

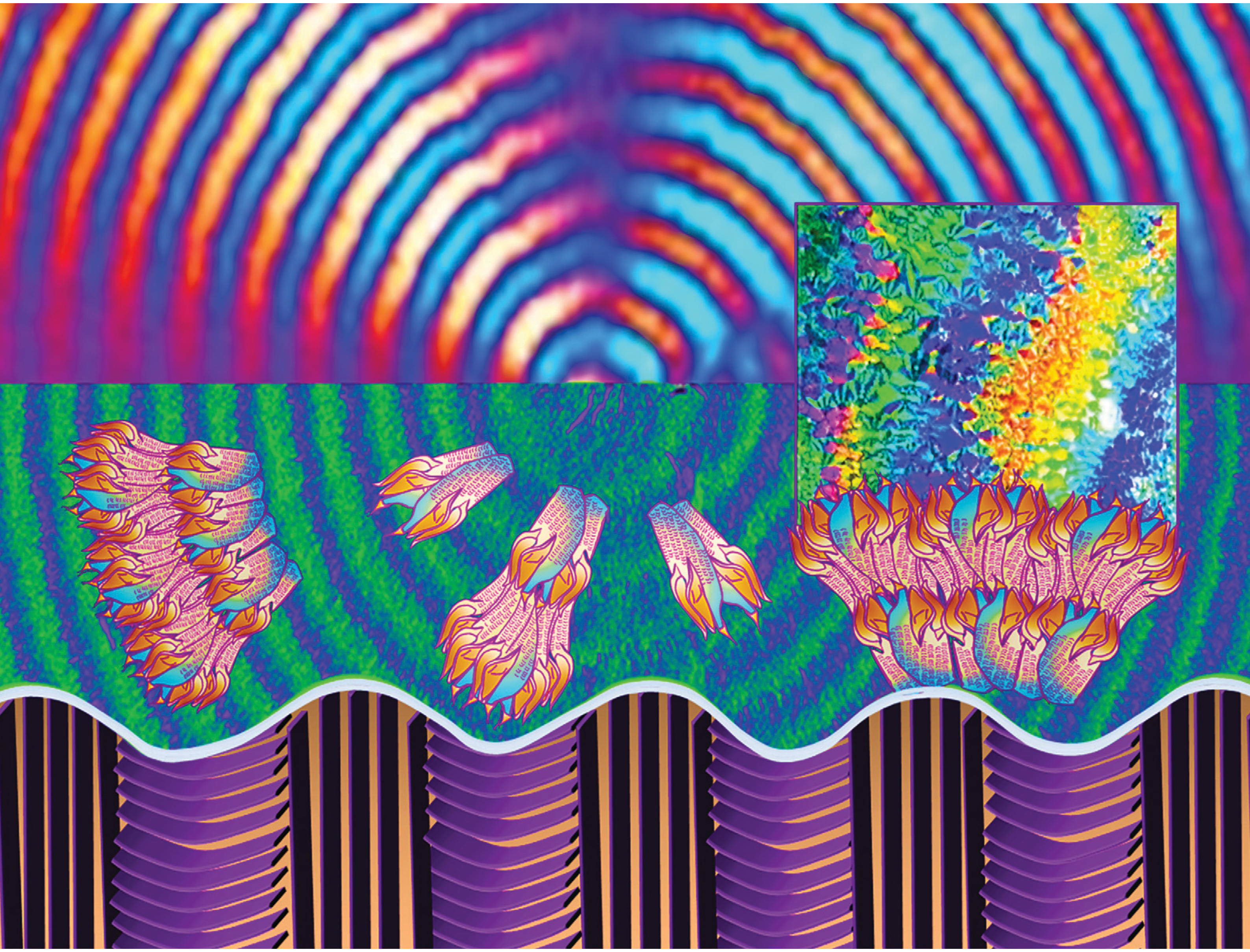

ISSN 1466-8033

ROYAL SOCIETY
OF **CHEMISTRY**

PAPER
Eamor M. Woo *et al.*
Universality in interior periodic assembly of banded D-(−)-poly(3-hydroxybutyrate) justified with the iridescence test

CrystEngComm

ROYAL SOCIETY OF CHEMISTRY

PAPER

View Article Online
View Journal | View Issue

Cite this: *CrystEngComm*, 2024, **26**, 1209

Received 7th December 2023,
Accepted 28th January 2024

DOI: 10.1039/d3ce01241g

rsc.li/crystengcomm

Universality in interior periodic assembly of banded D-(−)-poly(3-hydroxybutyrate) justified with the iridescence test†

Tzu-Ching Chuang,[a] Selvaraj Nagarajan,[a] Chean-Cheng Su,[b] Li-Ting Lee*[c] and Eamor M. Woo*[a]

The grating structure and periodic assembly in D-(−)-poly(3-hydroxybutyrate) (PHB), or simply poly(3-hydroxybutyrate), with diluent-modulated optical regularity are analyzed using microscopy techniques coupled with a unique 3D interior dissection technique. The top-surface valley band is a result of impingement of branching crystals evolving from normal-oriented main lamellar stalks, and the top-surface band is a result of the protruding lamellar stalks. The 3D dissection shows direct experimental proof of discontinuous interfaces between the successive bands, which are created by periodic impingement of neighboring lamellar bundles growing in the normal direction from the substrate. The iridescence phenomenon from the PHB periodic bands can be attributed to the grating-assembly structures with cross-bar pitches tuned to a suitable range by combination of diluents and temperature of growth, whose function resembles those seen in nature's iridescent crystals.

Introduction

Poly(β-hydroxybutyrate) (PHB) has been widely studied due to its biodegradability, and it is known that upon crystallization in a suitable temperature range, it displays periodic assembly, though not orderly patterns.[1–3] Like that in PHB, the formation of periodically banded spherulites (crystal aggregates) in many other semicrystalline polymers may be more complicated than those over-simply interpreted as the classical models of continuous helix-twist lamellae[4–9] taking a conformation like the classically well-known DNA molecular helices.[10] However, this classical proposition may be too simplified to be realistic; there might be more feasible alternatives for probing plausible formation mechanisms. It has been well known since a hundred years ago that small-molecule compounds often crystallize into periodic crystal aggregates,[11–15] just like those seen in semicrystalline long-chain polymers reported later in the literature in the past five decades. Yet, small-molecule compounds (organic or inorganic) do not have to chain-fold in order to pack into the basic hierarchical unit known as a lamella. However, many small-molecule organic or inorganic compounds are long known to display periodic optical-birefringence rings when viewed under polarized-light microscopy. Therefore, the fact that long-chain polymers undergo repetitive chain-folding in a lamella, and thus the consequence of chain-folding-induced surface stresses, is not sufficient or necessary conditions to account for the lamellae helix-twist (like a DNA macromolecule held by millions of pairs of base units).[10] This constrained proposition nevertheless has been used by some investigators for justifying mechanisms for periodic bands in polymeric spherulites. In all, the phenomenon of periodicity in crystal aggregates does not need more hard-to-justify propositions, but requires more experiment-justified breakthroughs for valid interpretations.

It is worth noting that many polymers or their blends may exhibit quite diverse morphologies upon crystallization, such as typical well-rounded Maltese-cross spherulites, straight-lamellae dendrites, hexagonal-shape,[16] feather-like spherulites,[17] and seaweed-like spherulites,[18] in addition to the widely-known periodic ring-bands. In some special cases, several different patterns co-evolve from a common center to form unique composite-face or Janus-face aggregates.[19,20] Thus, the complexity in assembly may defy simple or monotonous descriptive assumptions. Among these diversified patterns of crystal aggregates, periodic ring-

---

[a] *Department of Chemical Engineering, National Cheng Kung University, No.1, Tainan, 701-01, Taiwan. E-mail: emwoo@mail.ncku.edu.tw; Fax: +886 6 234 4496; Tel: +886 6 275 7575 x 62670*

[b] *Department of Chemical and Materials Engineering, National University of Kaohsiung, No. 700, Kaohsiung University Rd., Nan-Tzu Dist, Kaohsiung, 811, Taiwan*

[c] *Department of Materials Science and Engineering, Feng Chia University, Taichung, 407-24, Taiwan. E-mail: ltlee@fcu.edu.tw*

† Electronic supplementary information (ESI) available. See DOI: **https://doi.org/10.1039/d3ce01241g**

banded spherulites seen in many polymers have drawn the most attention; however, the formation mechanisms have remained quite controversial and highly debated among prevailing propositions. Yet, many of these propositions in the past decades have been difficult to solidly and experimentally prove without doubt, due to the small dimensions of constituent lamellae and extreme crowdedness of the aggregates. A recent study has shed new light that a periodic architecture can be composed of lamellae that branch or spawn new crystals periodically and some lamellae change their orientation alternately at periodic intervals, instead of propositions of continuous helix-twist lamellae.[21]

Newer approaches by interior 3D dissection[22–31] and synchrotron microbeam X-ray analysis[31,32] have been demonstrated to be useful for better insights of probing the crystal-assembly mechanisms. Earlier studies in the literature indicate that phase-separated domains in lamellae may confine and alter the arrangement of lamellae during aggregation of crystals. Therefore, phase separation with domain-confinement may strongly affect the birefringence types of spherulites, as demonstrated in poly(L-lactic acid) (PLLA).[16] Similarly, the PHB crystallization behaviour may change after addition of other amorphous polymers as diluents; that is to say, the morphology of PHB can be manipulated to display the desired crystal assembly patterns. The periodically banded morphology is very typical in PHB or its blends, as well as in many other semicrystalline polymers such as biodegradable poly(*p*-dioxanone) (PPDO),[32] and aliphatic polyesters, polyethylene (PE),[16,22,25–31,33–35] *etc.* Further observation of the inter-lamellar crevices in the periodically banded PHB by SEM microscopy techniques[30,31] has proved that PHB exhibits periodic bands composed of vertically-oriented lamellae and horizontally-oriented plates underneath the alternating ridge–valley bands. These breakthrough findings of the interior assembly[16,22,25–31,33–35] reported very different mechanisms from the conventional propositions[4–8] of periodic bands composed of continuous screw-like helix-twist lamellae simultaneously radiating out from a common center and all these lamellae, not only helix-twist, but also undergo synchronizing paces with an identical screw pitch. Such propositions of millions of continuous helix-twist lamellae possessing the same synchronized pitch require impractically stringent conditions (such as million pairs of gene-guided strong H-bonding in DNA-macromolecule screws) that may not be existent in common crystal plates. Crystallization and growth is controlled not just by thermodynamic but more by kinetic driving forces. Thermodynamic stability alone cannot possibly dictate all lamellae to display the same and precisely synchronized helix-twist conformation from nucleation all the way to completion. A typical spherulite can measure up to 30–300 μm in diameter or larger, but a discrete single-crystal lamella usually has a length not exceeding 5 μm or so, which hardly justifies the uninterrupted continuity from the nucleus to the periphery of a spherulite.

Neat poly(3-hydroxybutyrate) (PHB) (without blending with diluents) exhibits rough ring-bands at T_c = 40–100 °C;[30,31] the patterns are usually too rough to allow clear analyses on the top-surface or interior lamellar morphology *via* SEM characterization. A few recent studies[30,31] showed that the banding patterns are discretely assembled by two perpendicularly oriented crystal species in cross-hatch intersection, resembling a rib-strut structure with interior lamellae mutually intersecting at an angle ranging from 60 to 90°. Interestingly, such a grating structure in the banded PHB resembles nature's iridescent crystals. This work further probed the detailed morphology and assembly mechanisms by subjecting PHB to modulation with multiple diluent combinations of several suitable amorphous polymers that are known to be thermodynamically miscible with PHB. The objective was to search for the best modulation or regulation of crystal assembly in PHB for convenience of 3D dissection and trustworthy analyses leading to fundamental knowledge to establish an accountable interpretation of the existence of periodicity in crystal assembly.

Experimental

Materials and preparation

PHB, with T_g = 0.7 °C and T_m = 174 °C, was obtained from Polysciences, Inc. (USA). The M_w and PDI of PHB are 500 000 g mol^{-1} and 1.45, respectively. Poly(vinyl acetate) (PVAc), with T_g = 34.8 °C, was obtained from Scientific Polymer Products, Inc. (USA), with the M_w and PDI being 178 200 g mol^{-1} and 2.05, respectively. Poly(methyl acrylate) (PMA), with T_g = 7.3 °C, was obtained from Aldrich Chemical Company, Inc. (USA), with the M_w and PDI being 59 800 g mol^{-1} and 1.53, respectively. Dual diluents of PVAc and PMA were used as morphology modulation agents for PHB. Ternary PHB/PVAc/PMA blends were prepared by solution blending using chloroform ($CHCl_3$) as a co-solvent with a concentration of 4 wt% polymers in the solvent. For comparison, a different diluent was also used to prepare a binary blend with PHB. For this purpose, poly(1,3-trimethylene adipate) (PTA) was used, as PTA is known to be miscible with PHB. PTA was obtained from Scientific Polymer Products, Inc. (USA), with M_w = 8900 g mol^{-1}, PDI = 1.28, T_g = −63 °C, and T_m = 38 °C. Binary PHB/PTA samples were prepared using the same procedures as those for the ternary ones.

The polymer solution was cast on glass substrates and dried at 45 °C into thin-film samples with an average thickness = 20–30 μm. The dried film samples were then heated on a hot stage to the maximum melting temperature (T_{max} = 220 °C) for two minutes in order to erase prior crystals, and then rapidly removed to another hot stage pre-set at designed isothermal T_c till full crystallization. These crystallized samples were treated by solvent-etching using acetone and *p*-dioxane as the etching agent for 10 minutes in a sealed container at room temperature in order to wash out the amorphous polymer and imperfect crystals, and hence the etched specimens were considered to be more likely to reveal finer details in crystal assemblies.

Apparatus

Polarized-light optical microscopy (POM and OM). A polarized-light microscope (Nikon Optiphot-2, POM) equipped with a Nikon Digital Sight (DS-U1) digital camera and a CCD digital camera (NFX-35) was used in this work. For precise temperature control, a microscope hot stage (Linkam THMS-600 with a T_{95} temperature programmer) was used. A λ-tint plate (530 nm) was used to produce POM graphs with colored birefringence.

High-resolution field-emission scanning electron microscopy (HR-FESEM). HR-FESEM (Hitachi SU8010) was used for high-magnification microscopy characterization. Samples on glass substrates were fractured (cut with a diamond knife) and completed with solvent-etching and drying. Specimens were sputter-coated with platinum (10 mA, 300 seconds).

Differential scanning calorimetry (DSC). A differential scanning calorimeter (Perkin-Elmer, Diamond DSC) equipped with a mechanical intra-cooler for quenching was used. A heating rate of 20 °C min^{-1} was used with a nitrogen flow.

X-ray diffraction was performed using a 5 × 7 μm^2 microbeam at TPS-25A National Synchrotron Radiation Research Center (NSRRC, Hsin-Chu, Taiwan) with 15.03 keV photon energy. 2D-XRD patterns were recorded with a Dectris Eiger 1 M detector at 0.136 m (13.6 cm) distance and a q range of 0.179–113.41 Å, calibrated with cerium oxide in transition mode.

Results and discussion

Nano- to micro-structures in self-assembly of the surface-relief and interior morphology

Lee and Woo[30] in a pioneering study investigated correlations of thermal-induced cracks with interior assembly in neat PHB (with no diluents) that forms periodically banded aggregates. Although neat PHB does crystallize into ring-banded aggregates within a temperature range; however, the inter-band spacing tends to be very narrow and rings are quite corrupted with less regularity. For brevity, Fig. S1 (ESI†) shows POM graphs of neat PHB (without any diluents) crystallized at various T_c values (Fig. S1a–f†) in a wide temperature range of 60–100 °C. Except for the specimen of neat PHB at T_c = 70 °C with discernible regularity, all else show quite irregular ring patterns. Therefore, realistically, it would not be feasible to investigate the interior assembly based on neat PHB, which is the main reason that diluents were incorporated with PHB to modulate a clear ring pattern for feasibility of the study. This work further probed by utilizing an advanced methodology to render PHB to display more regular ring patterns for ease of analysis of lamellar assembly by interior dissection. It was found that if two amorphous polymers PVAc and PMA were used as combinatory diluents at a suitable ternary composition (adjusted by experiments), one was able to obtain more regular ring bands in PHB spherulites (crystallized from PHB/PVAc/PMA mixtures). PHB and PVAc have been known to be miscible as reported in the literature.[36,37] When crystallized at T_c = 100 °C, ternary PHB/PVAc/PMA (80/10/10) displayed the best morphological regularity, as shown in Fig. 1a–d. As long as the total amorphous contents are kept between 10 and 40 wt%, the adjustment of the amorphous contents in the PHB/PVAc/PMA blends does not appear to cause a significant difference in the banding morphology. All PHB blends show much more regular ring bands and wider inter-band spacing than neat PHB. Regular rings and wide inter-band spacing are ideal for SEM analysis by dissecting the interior assembly.

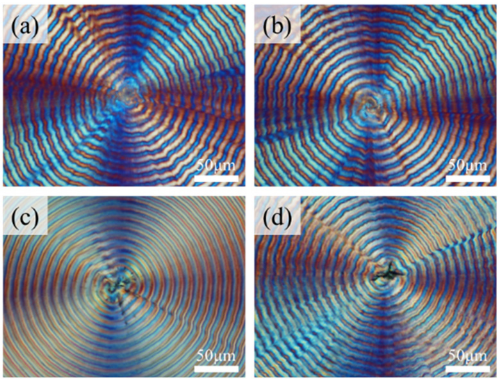

Fig. 1 POM graphs of PHB/PVAc/PMA blends crystallized at T_c = 100 °C of different ternary compositions: (a) 60/20/20, (b) 70/15/15, (c) 80/10/10, and (d) 90/5/5 [scale bar = 50 μm].

To confirm the miscibility in mixtures of PHB with PMA, DSC characterization was performed on several compositions of the ternary blend of PHB/PTA/PVAc. For brevity, DSC traces showing single composition-dependent T_g are demonstrated in Fig. S2 (ESI†). The numerical values of thermal properties of the PHB/PMA/PVAc blend are listed in Table S1 (ESI†). The DSC result shows that all ternary compositions of the polymer mixtures are miscible. Alternatively, a fixed ternary composition of PHB/PVAc/PMA = 80/10/10 was crystallized at various T_c values from 60–120 °C. For brevity, the POM characterization results are placed in Fig. S3 (ESI†), where Fig. S3a–c† show that at lower T_c = 60–80 °C, the ring bands are not quite regular; however, Fig. S3d–h† show that T_c = 90–110 °C leads to periodically banded spherulites with very regular patterns with the inter-band spacing being *ca.* 15–20 μm. Only at T_c exceeding 110 °C (T_c = 120 °C), the rings start to become corrupted. As a result, this work chose PHB/PVAc/PMA (80/10/10) fully crystallized at T_c = 105 °C as a model for in-depth morphology analysis and micro-beam X-ray analysis.

The topology of surface-relief patterns is usually masked by expelled impurities (molten species, amorphous polymers, *etc.*). Thus, appropriate etching treatments on specimens might be needed. Fig. 2a shows the SEM graphs for the top surface of the PHB/PVAc/PMA (80/10/10) blend crystallized at T_c = 105 °C. Fig. 2a shows the SEM image of a whole PHB

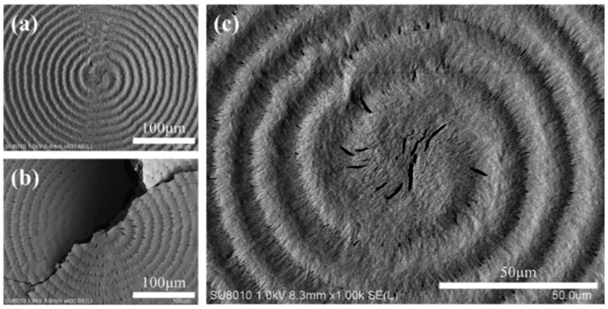

Fig. 2 SEM graphs for the top surface of the PHB/PVAc/PMA (80/10/10) blend crystallized at T_c = 105 °C: (a) un-etched image of the whole spherulite, (b) *p*-dioxane-etched image of the whole spherulite, and (c) zoomed-in image of the nucleus in (a).

spherulite without solvent etching, where fine textures of the top surface are hidden. Solvent-etching was conducted on crystallized specimens in order to expose the lamellar textures; however, solvent etching might induce cracks (Fig. 2b). Proper control of etching time was manipulated to obtain the best compromise. Fig. 2c shows the solvent-etched morphology of the top-surface banding patterns, where lamellae appear to evolve as a double spiral (spin in the clockwise direction) from a nucleus center. Cracks in the nucleus center are obvious, which are due to the fact that most of the nucleus sheaf-bundles are parallel and normal-oriented with respect to the substrate plane. Therefore, cracks, upon solvent etching, tend to align along the interfaces of sheaf-crystal bundles. A more careful examination can identify that cracks are not only in the nucleus center, but also on the ring bands. Interior dissection in later sections will expound this phenomenon.

Fig. 3 further shows zoomed-in micrographs to identify the detail of the surface-relief patterns of the periodic PHB spherulites crystallized from the ternary blend. Fig. 3a shows the whole PHB spherulite, where the top surface clearly displays periodic packing in repetitive cycles. The valley region is packed with tail-bending with spin pointing in the clockwise direction, which is in line with the double-spiral spin direction (clockwise direction). Apparently, the direction of tail-bending in the valley zone is well correlated with and perhaps determined by the lamellae spin direction. Fig. 3b and c show zoomed-in graphs of the ridge zone and valley zone, respectively. Radial-oriented cracks are present only in the ridge zone; by contrast, cracks are never seen in the valley zone. The valley zone is characterized only with lamellae tail-bending. The reason why cracks are present only in the ridge zone but not in the valley zone will become clear after interior-lamellae dissection analysis to be discussed in later sections.

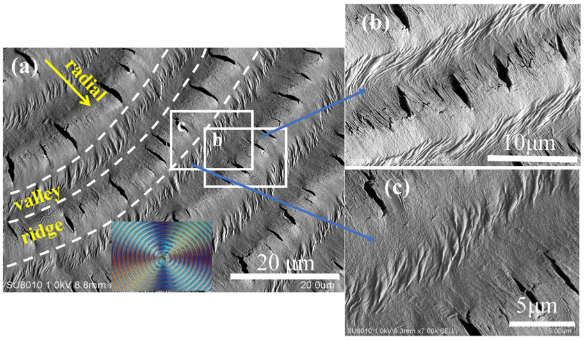

Fig. 3 SEM graphs for (a) the top surface of the PHB/PVAc/PMA (80/10/10) ternary blend crystallized at T_c = 105 °C; zoomed-in graphs of the (b) ridge zone and (c) valley zone.

3D assembly analysis by interior dissection

After the top surface analysis, interior 3D dissection was then attempted. PHB specimens were controlled to be fractured precisely across a spherulite along a radial direction, which was based on trials several times until success. Fig. 4 shows the SEM graph by interior 3D dissection of the PHB/PVAc/PMA (80/10/10) thickness-fractured film crystallized at T_c = 105 °C. The interior-dissected morphology clearly reveals periodic impingement (marked by white arrows) of the interior lamellae and their fractal-growth branches, which leads to periodic distinct interfaces that mark the boundaries between successive cyclic bands. White arrows mark the location of impingement between two neighbouring sets of growing lamellae. The interior lamellar rhythmic modulation perfectly matches with the periodic banding rhythm in the same pitches. Interestingly but not unexpectedly, the impingement pitch of the interior lamellae matches with the top-surface inter-band spacing (*ca.* 15–20 μm).

Fig. 5a shows the zoomed-in SEM graph for interior dissection of PHB/PVAc/PMA (80/10/10) crystallized at the same T_c = 105 °C. The tangential-oriented interfaces/cracks (white dashed lines) mark the periodic impingement of the interior lamellae, creating discontinuous interfaces aligned in the normal direction (tangential). Note that there are bundles of normal-oriented lamellae that evolve upward from the substrate; these normal-oriented lamellae initially slant

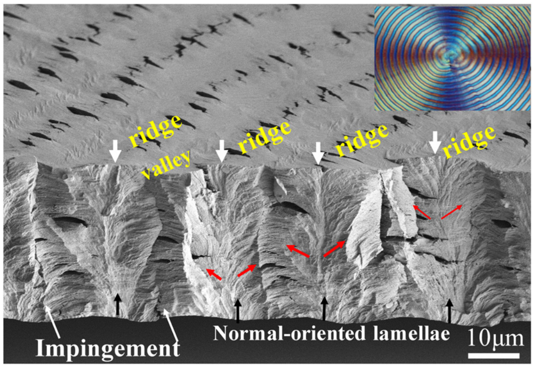

Fig. 4 SEM graph for interior dissection of PHB/PVAc/PMA (80/10/10) crystallized at T_c= 105 °C, revealing periodic impingement crevices of the interior lamellae, creating discontinuous interfaces (white arrows marking the periodic location of discontinuous interfaces created by lamellar impingement).

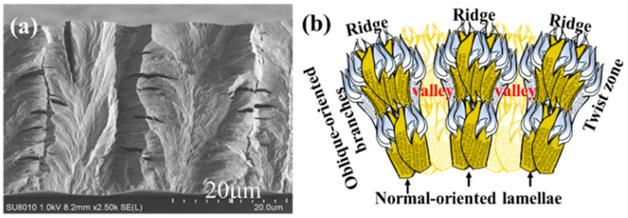

Fig. 5 (a) Zoomed-in SEM graph and (b) scheme for the interior normal-oriented lamellae evolving from the bottom substrate interface, for interior 3D dissection of PHB/PVAc/PMA (80/10/10) crystallized at T_c = 105 °C, revealing radial-oriented interfaces/cracks (short yellow lines) between horizontal lamellar bundles and tangential-oriented interface/cracks (long white dashed lines) by lamellar impingement.

at an oblique angle, and then bend further in the radial direction. These tail-bent lamellae are parallel and point in the radial direction. These radial-oriented lamellar bundles, upon detachment along the stress-prone interfaces between different species of crystal plates, create radial crevices/cracks (marked with yellow lines), which signify the pre-existing interfaces between the radial-oriented lamellae. These radial-oriented lamellae do not grow continuously or uninterruptedly; instead, they evolve from normal-oriented lamellae that are originally located periodically at a distance apart. Thus, when the radial-oriented lamellae grow to a matured length, they impinge with the neighbouring radial-oriented lamellae. As the growth of these lamellae is synchronized, they reach the impingement almost simultaneously at the same length and then impinge at the same time, creating a long tangential-oriented interface. Note again, the impingement pitch of the interior lamellae matches with the top-surface inter-band spacing (*ca.* 15–20 µm). Black dashed-lines mark the periodic location of impingement between two sets of lamellar bundles that are oriented from the bottom substrate and grow initially in the normal direction with accompanying fractal branches. The pitch of the interior lamellae perfectly matches with the periodic banding rhythm on the top surface. Apparently, the interior morphology of the banded PHB is not assembled as the classical propositions of continuous screw-like helix-twist lamellae pointing out from a common nucleus center.

In continuation, Fig. 5b shows the schematic for fractal-growth lamellae with side branches at oblique angles, till final impingement with interfaces. The mutual impingement of fractal-bundles of lamellae creates boundaries of discontinuities. The discussion focus is placed on revealing that the interior normal-oriented lamellae actually evolve from the substrate–specimen interface, where numerous branches grow sideward at 60–90° angles in two oblique directions. The mutual impingement of these two groups of sideward branches then creates distinct interfaces of discontinuities. Upward white arrows are used to mark the normal-oriented lamellae; downward white arrows mark a ridge zone on the top surface. The impingement of the two neighbouring groups of sideward branches, being nearly horizontal-oriented upon reaching the top surface, naturally appear to be flattened as a valley band.

For 3D dissection, interiors in all space aspects must be covered. After analysis of specimens fractured in the radial direction, circumferential-dissection was attempted. Again, several specimens were tested in trials till finding the best one. Here, the term “circumferential’ means along the circular rim of a certain circular band that happened to be fractured. Interior dissection analysis provides a unique opportunity to examine how lamellae go through a transition from top-surface ridges to valleys. Obviously in previous top-surface SEM micrographs, it was not possible to discern how lamellae self-assemble in zones from ridges to valleys, as all top-surface lamellae are highly jammed and crowded. The dissected interiors, however, provide a much clearer view for such a purpose. Fig. 6 shows the SEM graphs of the fractured surface of PHB/PVAc/PMA (80/10/10) crystallized at T_c = 105 °C, which was fractured in the circumferential direction of circular bands. A specific spot was zoomed-in at a greater magnification on a ridge zone (Fig. 6a1), where the interior lamellae underneath the ridge are all normal-oriented and parallel-bundled, with each bundle showing an individual thickness of *ca.* 0.5 µm. By comparison, the interior lamellae underneath the valley are all horizontal (radial)-oriented and parallel-bundled (Fig. 6a1), with each bundle showing an individual thickness slightly thinner at *ca.* 0.2–0.4 µm. Fig. 6b shows a schematic for picturing the circumferential-fractured surface of a PHB ring-banded spherulite at T_c = 105 °C. A zoomed-in image of a valley zone of the banded PHB is to be discussed subsequently in the next figure.

Furthermore, several spots of the interiors were examined for universality. Fig. 7a shows the ow-mag. SEM micrograph of circumferential-fractured interiors of PHB/PVAc/PMA (80/10/10) crystallized at T_c = 105 °C. Fig. 7a1 shows the zoomed-in image for the interior lamellae that are located directly underneath a transition zone from ridges crossing into valleys (images stacked to cover the wider zone). The schematic (inset at upper right) exemplifies the valley zone

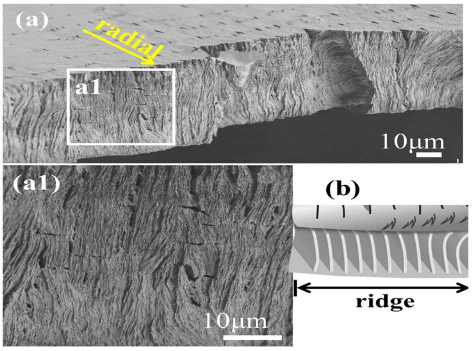

Fig. 6 (a) SEM graphs of the fractured surface of PHB/PVAc/PMA (80/10/10) crystallized at T_c = 105 °C; zoomed-in image of (a1) a ridge zone and (b) schematic for a ridge zone in the circumferential-direction fractured surface of the PHB ring-banded spherulite at T_c = 105 °C.

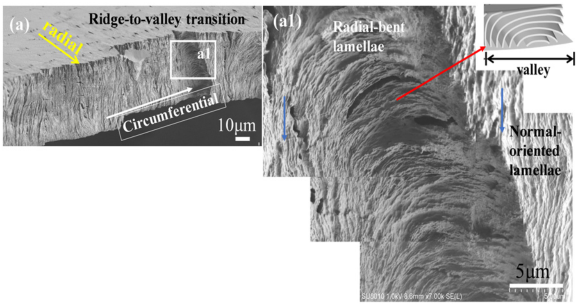

Fig. 7 (a) SEM graphs of circumferential-fractured interiors of PHB/PVAc/PMA (80/10/10) crystallized at T_c = 105 °C and (a1) zoomed-in image of interior lamellae underneath the transition zone of ridges to valleys.

showing bent lamellae in the circumferential-direction. The lamellae just underneath the valley zone are all radially oriented with an inverted "U"-bend (*i.e.*, convex). Directly adjacent to the radially (horizontally) oriented lamellae are the normal-oriented lamellar bundles (marked with blue arrows). The left-hand-side of the zoomed-in SEM graph in Fig. 7a1 shows that as the initially normal-oriented lamellae (underneath a ridge) approach the valley zone, they bend and twist into an inverted "U"-shape (underneath a valley). The assembly repeats similarly and repetitively on the other right-hand side of the valley to start a new cycle.

For the top surface of banded PHB, further evidence is displayed to prove the existence of discontinuity from band to band created by lamellae's sudden change of direction from the radial direction to a tangential one, rather than the conventional thought of a gradual linear screw-like helix twist in the radial direction. Fig. 8a and b show the SEM micrograph and scheme for periodic bands as viewed on the top surface of banded PHB. The SEM images on the top-surface bands support the interior 3D dissection that the band-to-band transition is discontinuous, with the lamellae being assembled alternately in the radial direction and then a sudden change to the tangential direction. An AFM phase image, adapted and taken from an earlier study,[31] is re-used here for further supporting the evidence given in the SEM characterization on the top surface of the ridge–valley transition.

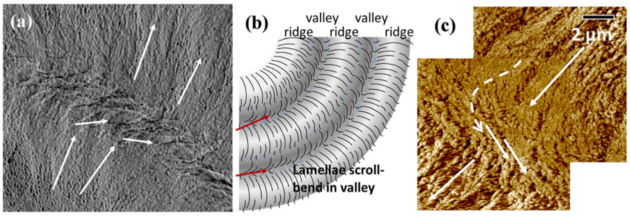

Fig. 8 Topology at the valley/ridge transition zone as viewed in (a) the SEM graph for the top surface (of PHB crystallized from PHB/PVAc/PMA) and (b) the scheme for top-surface bands, and (c) the AFM phase image [PHB/PTA (75/25)] at T_c = 60 °C (in this figure, PHB was diluted by 25 wt% poly(trimethylene adipate) (PTA).

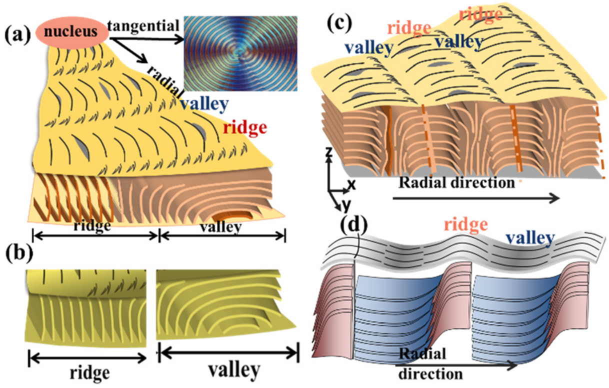

Fig. 9 Schematic illustration for (a and b) the circumferential-direction fractured surface, (c) inter-bundle impingement (blue dashed lines marking the impingement), and (d) abrupt twist from flat-on to edge-on orientation near the end of a pitch of the PHB ring-banded spherulite at T_c = 105 °C (PHB crystallized from the PHB/PVAc/PMA blend).

To view the universal mechanisms of crystal assembly leading to periodic bands, we combine the results of the assembled lamellae underneath the ridge and valley zones, respectively. Fig. 9a and b show generalized schemes (fractured along the circumferential direction) revealing the correlation of periodicity on the top surface *vs.* interiors of PHB crystallized at T_c = 105 °C. The circumferential-fractured interior displays periodic lamellae being self-assembled in alternate normal-to-horizontal orientation changes, just like that observed in the radial-fractured interiors. Consistency in 3D dissection suggests a universal feature of lamellar assembly leading to similar periodic architectures. By contrast, when fractured along the radial direction (instead of the circumferential one), a different view on discontinuity can be exposed. Schematic illustrations for two different common modes of creating an inter-band discontinuity: impingement of inter-bundles *vs.* sudden twist of same lamellae. Fig. 9c and d show generalized schemes for illustrating two different modes of creating an inter-band

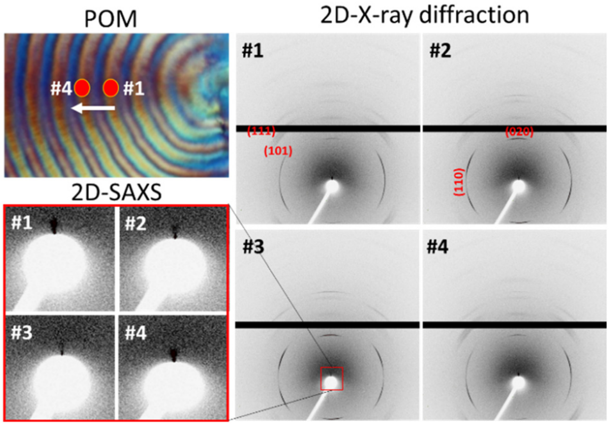

Fig. 10 Positioning of the PHB spherulite in the POM micrograph with respect to the incident microbeam and 2D X-ray diffraction patterns (SAXS and WAXD) recorded in rings at spot locations #1 to #4.

discontinuity: (a) inter-bundle impingement (blue dashed lines marking the impingement) and (b) lamellae sudden twist from flat-on to edge-on orientation near the end of a pitch. Emphatically for the assembly shown in graph-b, the lamellae do twist but the twist is not a 360°-angle rotating continuously as a screw-like helix, but rather a 90° twist from edge-on to flat-on, and the growth cycle ends. A new cycle repeats the same way. These two schemes (a and b) both represent two common ways of correlation of the top-surface pattern with interior lamellae assembly, and such a grating cross-hatch is responsible for the periodic optical rings as viewed in POM. The difference of these two modes lies on mainly how the interior lamellae self-assemble periodically to create periodic ridge to valley zones.

Fig. 10 depicts a trend illustrating the modulation of X-ray diffraction intensity across various crystal planes (indicated in the *y*-axis). This modulation corresponds to the sequential movement from the central point of one ridge to the other ridge. The intensity of crystals is intricately linked to the arrangement patterns of lamellae and unit cells. Oscillations in the crystal-plane intensity signify both parallel and perpendicular orientations concerning the micro-beam axis within the ridge-to-valley distance. The manifestation and cessation of diffraction signals hinge upon the precise alignment of the crystal planes and lamellae in relation to X-ray incidence, whether parallel or perpendicular. In the ridge zone, robust signals are emanated from crystal planes such as (111) and (101), and SAXS for lamellar orientations. Conversely, the valley region exhibits distinctive signals corresponding to the (020), (130), and (040) planes. Furthermore, the signals of the (110) planes manifest in both ridge and valley areas (ESI† Fig. S4). Significantly, the presence of the signal of the (020) crystal plane in the valley region suggests prevalence of flat-on crystals, while the appearance of the signal of the (101) crystal planes on the ridges corresponds to the *ac*-axis crystal plane, confirming an abundance of edge-on crystals. The two-dimensional plot of SAXS in Fig. 10 underscores the maximal intensity difference of X-ray signals in a radial direction within the ridge-to-ridge distance. Derived from the one-dimensional correlation function in Fig. S5,† the estimated long-period is L_o = 84 Å, with a crystal thickness (L_c) measuring 35 Å and an amorphous thickness (L_a) of 47 Å for the PHB/PVAc/PMA banded spherulite. Significantly, the 2D SAXS signals reinforce the observed lamellar alignment in the WAXD crystal signals, which collectively are experimentally supported by the SEM interior-dissection morphology discussed earlier.

Iridescence of neat PHB *vs.* PHB/PVAc/PMA blends

In nature, photonic interference with sunlight is a common phenomenon and can be commonly seen in many bio-species or crystalline minerals.[38–41] In addition to many nature's bio-species, iridescence is one of the most magical optical effects seen in many gemstones, which are inorganic crystals formed by nature through crystallization and self-assembly from molten molecules. A handy example is inorganic opals (SiO_2 micro-spheres). Synthetic polymers, upon super-molecular self-assembly by crystallization, liquid-crystalline order, or phase separation, *etc.*, may display similar photonic-iridescence phenomena and have been documented in the literature.[42–44] Aside from the assembly by crystallization, polymers in thin films can be altered into specific micro-patterns to display iridescence, which imprint wrinkled surfaces using techniques such as flexible and rigid bilayer-sandwiching,[45] solvent swelling,[46] thermal heating,[47] stretching,[48,49] strain by a cross-linking agent,[50] *etc.* Nevertheless, techniques of wrinkled textures are fabricated to take wavy patterns on topology, which might inevitably cause side effects of period-doubling, defects in folds, or different types of undesirable or unavoidable wrinkles.[51,52]

For nature's organic living species (plants and animals), their functional iridescence is tuned in million years of evolution to the most suitable nano- or micro-structures. In this work, we demonstrate novel techniques for polymers to display fine-tuned assemblies by using diluents in crystallization as morphology modulation. Orderly-assembled crystals may display interference of white light if the scales of periodic order are near or within the visible-light wavelengths. Neat PHB displays ring bands but does not possess clear order, which however, can be tailor-made by introducing suitable modulating agents.

By comparison with the miscible diluent-modulated PHB (diluted by amorphous PVAc and PMA), iridescence of neat PHB specimens at various T_c values was also tested, and is shown in Fig. 11. Test set-ups for interference with white light are similar to those in previous work.[31] Obviously, the neat PHB specimens (with no diluents), upon crystallization at T_c = 65–100 °C, all display corrupted ring bands (highly irregular rings) and lead to non-iridescence, although some weak iridescence is barely visible but not comparable to those in the PHB/PVAc/PMA systems. This proves that PHB, only when properly modulated with diluents and tailor-made, can take orderly microstructures to perform iridescence functions. If crystallized at an even lower T_c such as 30 °C,

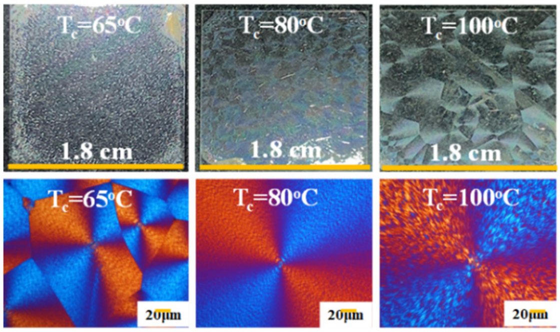

Fig. 11 Non-iridescence or weak iridescence of neat PHB with irregular bands crystallized at T_c = 65 °C, 80 °C, and 100 °C, respectively (left to right).

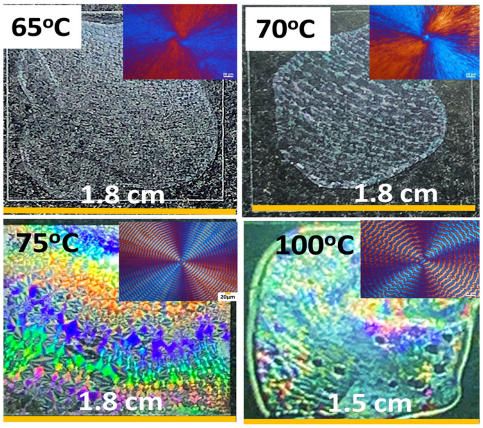

Fig. 12 (Top row) non-iridescence for specimens with no rings at T_c = 65 °C and 70 °C *vs.* (bottom row) intensified iridescence of regularly banded PHB crystallized from PHB/PVAc/PMA (80/10/10) at 75 °C and 100 °C.

neat PHB is totally ringless with small sizes of spherulites, which are not expected to display effective light interference.

Neat PHB displays irregularly rough ring bands at T_c = 65–100 °C with no clear order, which however, can be tailor-made into orderly patterns by introducing suitable modulating agents. As discussed above, neat PHB crystallized at low T_c displayed barely discernible ring bands and weak iridescence. Yet, introduction of modulating miscible diluents such as PVAc and PMA (both non-crystalline) into PHB crystallized at the same range of T_c = 65–100 °C led to periodic orderly bands. Fig. 12 shows the dramatic effect of morphology modulation on capacity for iridescence properties. At T_c = 65 °C, although the banding pattern of PHB/PVAc/PMA (80/10/10) is slightly better in regularity than that of neat PHB at the same T_c, it is still not perfect (inset POM on the upper left corner), and iridescence is visible but not intense (top row of Fig. 12). By comparison, the periodic morphology becomes totally different to display orderly ring bands leading to effective white-light interference and intense iridescence (bottom row of Fig. 12). At T_c = 100 °C or higher, the banding pattern of PHB/PVAc/PMA (80/10/10) starts to become corrupted and irregular, and the iridescence is still visible but becomes less intense than that of the specimen crystallized at T_c = 75 °C.

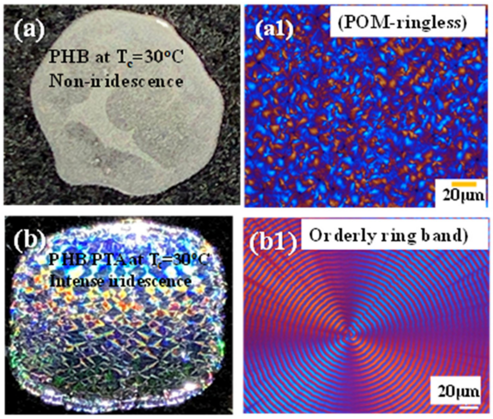

Fig. 13 Effect of morphology modulation of ring regularity on iridescence: (a) non-iridescence, (a1) POM graph with ringless spherulites of neat PHB *versus* (b) intense iridescence, (b1) POM graph with orderly ring bands of the PHB/PTA (80/20) blend. Both systems crystallized at the same T_c = 30 °C.

Fig. 13 shows the side-by-side comparison of non-iridescence from ringless PHB spherulites of neat PHB *versus* intense iridescence from orderly bands crystallized from the PHB/PTA (80/20) blend (both crystallized at T_c = 30 °C). Obviously, no orderly grating microstructures are present in ringless PHB spherulites, which expectedly display non-iridescence (Fig. 13a1). By contrast, intense iridescence is seen in orderly ring bands of the PHB/PTA (80/20) blend, which is in agreement with the previous result for the regularly banded PHB crystallized from PHB/PVAc/PMA (80/10/10) at 75 °C and 100 °C.

Thermodynamically, it is an unlikely stringent condition to maintain a synchronized identical helix pitch for millions of lamellae radiating simultaneously outward from a common nucleus, considering that these lamellar crystals, unlike DNA molecules, do not possess gene-guided molecular structures with millions of pairs of base units for H-bonding that are fundamental for holding continuously stable helices along the same molecular axis. It should be emphasized on a crystal key feature. Even though the thousands of lamellae were assumed to be capable of individually helix-twisting; however, they still would not display clear optical bands if these helix-twist plates were not synchronized in a perfect pace with the same pitch. Any miss-matching or offsets of the helix pitches simply would result in extinction of birefringence, as one should always bear in mind that the light does not interact with only a single lamella, but with hundreds of pitch-offset lamellae in stacked bundles across the entire film thickness. Kinetically, on the other hand, it would be more plausible that growth of crystals and their re-orientation or deformation (such as twisting or scrolling) can be modulated to be in a synchronized pace intermittently. Such assembly with periodic modulation of growth leads to a grating structure. Obviously, the PHB ring bands (as viewed in the POM and SEM evidence) are constructed by periodic grating assembly of discrete crystals self-packed as fractal branches along with their parental main stalk lamellae.

Conclusions

Grating with micro- to nano-scale hierarchical assemblies is common in nature's structural photonic crystals for performing light interference. Such grating assembly is also proved in PHB crystallized with periodic bands. However, neat PHB displays rough and irregular ring bands, leading to weak iridescence; the microstructures of PHB, however, can be tailor-made by introducing suitable diluents, which are capable of modulating the regularity and periodicity of the grating-banded patterns for displaying more intense iridescence. Periodically banded PHB spherulites are modulated by mixing with suitable diluents; in this work, dual polymeric diluents PVAc and PMA are intentionally introduced for more precisely regulating the assembly regularity for correlation with iridescence.

Unique 3D morphology interior dissection was conducted to expose the lamellar architectures on surfaces and in the interior. A grating assembly with cross-hatch fractal growth of periodic branches is confirmed, where a "pitch" of a periodic band (as seen in the fractured interiors *via* SEM evidence) is in perfect match with the optical inter-band spacing. Conventional propositions of continuous helix-twist lamellae for periodic optical bands are re-examined and testified with solid experimental observations.

The unique 3D dissection technique allows direct experimental proof of discontinuous interfaces between the successive bands, which are created by periodic impingement of neighbouring lamellar bundles growing in the normal direction from the substrate. The valley band on topology exhibits a discontinuous interface that is a result of impingement of the crystals of slant-angle-oriented branches originally evolving from the interior normal-oriented main lamellar stalks; by contrast, the ridge band is a result of the protruding normal-oriented lamellar stalks. In the ring-banded PHB spherulites, all "lamellae" (branches or main stalks) are not in helix-twist conformation; instead, they are assembled by discrete single-crystals. For continuous helix-twist propositions to work in accounting for the periodic optical rings, thousands of interior lamellae must helix-twist in a perfectly synchronized pace, and each of the screw-like helical plates' conformation must be firmly held by strong forces of H-bonding. Obviously, both molecular requirements are absent in the crystal plates.

The periodic assembly of discrete crystals self-packed as fractal branches along with their parental main-stalk lamellae, leading to a grating structure, which possesses nano- to micro-architectures effective for interference with white light. By using a chiral biodegradable polyester, PHB modulated with suitable diluents, critical light is shed on understanding the crystal self-assembly leading to hierarchical periodicity that has long intrigued the science community. Such periodic assemblies with nano-gratings can display iridescence.

Author contributions

T. C. Chuang (grad. student at this work) was involved in data curation; S. Nagarajan (Post-doctoral Research Associate) helped in analysis and developing in-depth schemes; C. C. Su and L. T. Lee co-contributed to supervising the group research work; E. M. Woo (Professor) secured funding, initiated original research ideas, and was in charge of writing and polishing the final texts.

Conflicts of interest

There are no conflicts to declare.

Acknowledgements

The authors acknowledge the research grants (NSTC 112-2221-E-006-009-MY3) from Taiwan's National Science and Technology Council (NSTC). S. Nagarajan is grateful for a Research Fellowship from the Taiwan government.

Notes and references

1 H. Mitomo, P. J. Barham and A. Keller, *Polym. J.*, 1987, **19**, 1241–1253.
2 P. J. Barham, A. Keller, E. L. Otun and P. A. Holmes, *J. Mater. Sci.*, 1984, **19**, 2781–2794.
3 S. J. Organ and P. J. Barham, *J. Mater. Sci. Lett.*, 1989, **8**, 621–623.
4 T. Ikehara and T. Kataoka, *Sci. Rep.*, 2013, **3**, 1444.
5 B. Lotz and S. Z. D. Cheng, *Polymer*, 2005, **46**, 577–610.
6 A. Toda, K. Taguchi and H. Kajioka, *Macromolecules*, 2008, **41**, 7506–7512.
7 M. Kunz, M. Drechsler and M. Möller, *Polymer*, 1995, **36**, 1331–1339.
8 M. Rosenthal, G. Portale, M. Burghammer, G. Bar, E. T. Samulski and D. A. Ivanov, *Macromolecules*, 2012, **45**, 7454–7460.
9 M. Rosenthal, M. Burghammer, G. Bar, E. T. Samulski and D. A. Ivanov, *Macromolecules*, 2014, **47**, 8295–8304.
10 R. F. Peter Atkins and Julio de Paula, *Physical Chemistry: Quanta, Matter, and Change*, Oxford University Press, 11th edn, 2014.
11 A. G. Shtukenberg, Y. O. Punin, A. Gujral and B. Kahr, *Angew. Chem., Int. Ed.*, 2014, **53**, 672–699.
12 E. Gunn, R. Sours, J. B. Benedict, W. Kaminsky and B. Kahr, *J. Am. Chem. Soc.*, 2006, **128**, 14234–14235.
13 T.-Y. Chen, E. M. Woo and S. Nagarajan, *Sci. Rep.*, 2020, **10**, 4062.
14 T.-Y. Chen, E. M. Woo and S. Nagarajan, *CrystEngComm*, 2020, **22**, 467–477.
15 J. S. Bangsund, T. R. Fielitz, T. J. Steiner, K. Shi, J. R. Van Sambeek, C. P. Clark and R. J. Holmes, *Nat. Mater.*, 2019, **18**, 725–731.
16 Y. T. Yeh and E. M. Woo, *Macromolecules*, 2018, **51**, 7722–7733.
17 K. C. Yen and E. M. Woo, *Polym. Bull.*, 2009, **62**, 225–235.
18 I. H. Huang, L. Chang and E. M. Woo, *Macromol. Chem. Phys.*, 2011, **212**, 1155–1164.
19 Y. H. Mandala, E. M. Woo, H. Ni'mah and S. Nurkhamidah, *Polymer*, 2019, **176**, 168–178.
20 Y.-L. Tseng, K.-N. Chuan and E. M. Woo, *Ind. Eng. Chem. Res.*, 2020, **59**, 7485–7494.
21 E. M. Woo and G. Lugito, *Eur. Polym. J.*, 2015, **71**, 27–60.
22 G. Lugito and E. M. Woo, *Cryst. Growth Des.*, 2014, **14**, 4929–4936.
23 C. H. Tu, E. M. Woo and G. Lugito, *RSC Adv.*, 2017, **7**, 47614–47618.

24 S. Nagarajan and E. M. Woo, *ACS Appl. Mater. Interfaces*, 2021, **13**, 41200–41208.

25 G. Lugito, C. Y. Yang and E. M. Woo, *Macromolecules*, 2014, **47**, 5624–5632.

26 E. M. Woo, W.-T. Tsai and G. Lugito, *Macromolecules*, 2017, **50**, 283–295.

27 S. Nagarajan, E. M. Woo, C. Su and C. Yang, *Macromol. Rapid Commun.*, 2021, **42**, 2100202.

28 S. Nagarajan and E. M. Woo, *Macromol. Rapid Commun.*, 2021, **42**, 2000708.

29 S. Nagarajan, *Macromol. Rapid Commun.*, 2021, **42**, 2100359.

30 M. S. Lee and E. M. Woo, *Polymer*, 2019, **166**, 88–97.

31 Y. Liao, S. Nagarajan, E. M. Woo, W. Chuang and Y. Tsai, *Macromol. Rapid Commun.*, 2021, **42**, 2100281.

32 S. Nagarajan, K. Huang, W. Chuang, J. Lin and E. M. Woo, *J. Phys. Chem. C*, 2023, **127**, 2628–2638.

33 G. Lugito and E. M. Woo, *J. Polym. Sci., Part B: Polym. Phys.*, 2016, **54**, 1207–1216.

34 S. Nagarajan and E. M. Woo, *ACS Appl. Mater. Interfaces*, 2021, **13**, 41200–41208.

35 E. M. Woo, L.-Y. Wang and S. Nurkhamidah, *Macromolecules*, 2012, **45**, 1375–1383.

36 L. Chang, Y.-H. Chou and E. M. Woo, *Colloid Polym. Sci.*, 2011, **289**, 199–211.

37 Y. An, L. Dong, L. Li, Z. Mo and Z. Feng, *Eur. Polym. J.*, 1999, **35**, 365–369.

38 S. Kinoshita, S. Yoshioka, Y. Fujii and N. Okamoto, *Forma*, 2002, **17**, 103–121.

39 S. Kinoshita, S. Yoshioka and J. Miyazaki, *Rep. Prog. Phys.*, 2008, **71**, 076401.

40 G. S. Smith, *Am. J. Phys.*, 2009, **77**, 1010–1019.

41 S. Vignolini, P. J. Rudall, A. V. Rowland, A. Reed, E. Moyroud, R. B. Faden, J. J. Baumberg, B. J. Glover and U. Steiner, *Proc. Natl. Acad. Sci. U. S. A.*, 2012, **109**, 15712–15715.

42 E. M. Woo, K. C. Yen, Y. T. Yeh and L. Y. Wang, *Macromolecules*, 2018, **51**, 3845–3854.

43 D. P. Song, G. Jacucci, F. Dundar, A. Naik, H. F. Fei, S. Vignolini and J. J. Watkins, *Macromolecules*, 2018, **51**, 2395–2400.

44 P. Liu, X. Guo, F. Nan, Y. Duan and J. Zhang, *ACS Appl. Mater. Interfaces*, 2017, **9**, 3085–3092.

45 C. H. Lin, C. Y. Huang, J. Y. Ho and H. Y. Hsueh, *ACS Appl. Mater. Interfaces*, 2020, **12**, 22365–22377.

46 J. Y. Chung, A. J. Nolte and C. M. Stafford, *Adv. Mater.*, 2009, **21**, 1358–1362.

47 N. Bowden, S. Brittain, A. G. Evans, J. W. Hutchinson and G. M. Whitesides, *Nature*, 1998, **393**, 146–149.

48 S. P. Lacour, S. Wagner, Z. Huang and Z. Suo, *Appl. Phys. Lett.*, 2003, **82**, 2404–2406.

49 P. Kim, M. Abkarian and H. A. Stone, *Nat. Mater.*, 2011, **10**, 952–957.

50 E. P. Chan, E. J. Smith, R. C. Hayward and A. J. Crosby, *Adv. Mater.*, 2008, **20**, 711–716.

51 B. H. Kim, Y. Choi, J. Y. Kim, H. Shin, S. Kim, S. W. Son, S. O. Kim and P. Kim, *Adv. Mater.*, 2014, **26**, 4665–4670.

52 H. Y. Hsueh, M. S. Chen, C. Y. Liaw, Y. C. Chen and A. J. Crosby, *ACS Appl. Mater. Interfaces*, 2019, **11**, 23741–23749.